High Sensitivity of Human Translesion DNA Synthesis Polymerase κ to Variation in O^6-carboxymethylguanine Structures

Michael H. Räz[‡], Emma Sandell[‡], Kiran Patil[†], Dennis G. Gillingham[†], and Shana J. Sturla[‡,*]

[‡]Department of Health Sciences and Technology, ETH Zürich, Schmelzbergstrasse 9, Zürich, 8092, Switzerland

[†]Department of Chemistry, University of Basel, St. Johanns-Ring 19, Basel, 4056, Switzerland

ABSTRACT: Carboxymethylation of DNA, including the formation of the DNA adduct O^6-carboxymethylguanine (O^6-CMG) is associated with lifestyle factors, such as diet. It can impede replicative polymerases (Pols) and lead to replication fork stalling, or an alternative means for replication to proceed by translesion DNA synthesis (TLS). TLS requires specialized DNA Pols characterized by open and preformed active sites capable of preferential bypass of alkylated DNA adducts, but that have high error rates, leading to mutations. Human TLS Pols can bypass O^6-CMG with varying degrees of accuracy, but it is not known how the chemical structure of the O^6-CMG adduct influences polymerase proficiency or fidelity. To better understand how adduct structure determines dNTP selection at lesion sites, we prepared DNA templates with a series of O^6-CMG structural analogs and compared the primer extension patterns of Y- and X-family Pols in response to these modifications. The results indicate that the structure of the DNA adduct had a striking effect on dNTP selection by Pol κ and that an increased steric size influences the fidelity of Pol η, whereas Pol ι and β function were only marginally affected. To test the hypothesis that specific hydrogen bonding interactions between the templating base and the incoming dNTP are a basis of this selection, we modeled the structural analogs with incoming dNTP in the Pol κ active site. These data indicate that the base pairing geometry and enhanced stabilization through a dense hydrogen bonding pattern are important molecular features in the dNTP incorporation fidelity of Pol κ. The study provides a basis for understanding error-free bypass of O^6-CMG by Pol κ and illustrates that the Pol relies strongly on hydrogen-bond complementarity for nucleotide selection.

INTRODUCTION

Strong electrophiles are potent genotoxins, damaging the structure of DNA and forming covalent DNA adducts.[1] DNA damage that is left unrepaired can contribute to genomic instability, disrupt cellular functions and ultimately lead to diseases, including cancer.[1] Carcinogenesis is characterized by an accumulation of somatic mutations, often caused by genotoxic chemicals such as *N*-nitroso compounds (NOCs).[2, 3] NOCs are present in meat,[4] tobacco smoke, fuel combustion products[5, 6] and also are produced endogenously in the stomach and large intestine.[7, 8] Their metabolic activation gives rise to reactive alkylating agents, which can modify exocyclic oxygen- and ring nitrogens in DNA.[9] However, the formation of O^6-alkylguanine adducts is of particular concern due to their strong miscoding potential during DNA synthesis, where DNA polymerases (Pols) tend to misincorporate T, resulting in GC→AT mutations.[10, 11]

Colorectal cancer (CRC) is characterized by the sequential accumulation of mutations in tumor suppressor- and proto-oncogenes,[12, 13] with point mutation hot-spots located in the *kirsten rat sarcoma (KRAS)* gene and comprised of GC→AT single base substitutions in up to 50% of colon cancers.[14, 15] Amongst pro-mutagenic O^6-alkylguanine adducts, O^6-carboxymethylguanine (O^6-CMG) may contribute to GC→AT and GC→TA mutation patterns observed in human CRC tumors.[16, 17] Furthermore, high O^6-CMG levels were measured in DNA from human colon cells[18, 19] and in the sigmoid colon and rectum.[20] In addition, increased O^6-CMG adduct levels in colon cells have also been linked to diets high in red meat.[19-22] Consuming high levels of red meat is hypothesized to facilitate the gastrointestinal bacterial nitrosation of glycine, thereby forming diazoacetate intermediates with the potential to transfer carboxymethyl-groups to nucleobases.[7, 8] Despite the correlation between red meat, O^6-CMG, and CRC, no direct biological evidence between the occurrence of O^6-CMG and mutations driving colon carcinogenesis have been established. Detailed knowledge about the enzymatic processing of O^6-CMG will be crucial in determining its relevance in the initiation and progression of colon cancer and in establishing biomarkers of CRC risk. Even more, O^6-CMG stands out amongst DNA alkylation adducts as one of the few reported negatively charged (COO-) DNA adducts [23, 24] under physiological conditions.

Recent studies assessed the biological effects of unrepaired O^6-CMG during DNA replication in polymerase bypass studies with translesion DNA synthesis (TLS) Pols deficient cell lines or isolated Pols. In HEK293 cells transfected with plasmids containing a site-specific O^6-CMG, the adduct was a modest block for DNA synthesis and was moderately mutagenic.[25] Adduct bypass decreased in cells deficient in Pol κ and ζ and O^6-CMG induced exclusively GC→AT mutations at a frequency of 6.4% when Pol ι was

genetically depleted.[25] Therefore, the data suggested an involvement of TLS Pols κ and ζ in error-free bypass of O^6-CMG whereas Pol ι seems to be responsible for the mutagenic bypass of the adduct.[25] In line with these findings, primer extension experiments demonstrated that the replicative Pol δ was only moderately blocked. Additionally, Pol κ, which only inserted dCTP, was the highest fidelity Pol amongst the TLS Pols tested,[26] and Pols η and ι frequently misincorporated dATP and dTTP opposite O^6-CMG.[26] Interestingly, the high rate of dATP insertion opposite O^6-CMG by Pol η contradicted results in transfected cells, where Pol η appeared to have no function in O^6-CMG bypass. Overall, the data from both isolated enzymes and cells suggest the miscoding potential of O^6-CMG depends on which Pol is functional in the TLS bypass of O^6-CMG and its mechanism of processing the adduct.[25, 26]

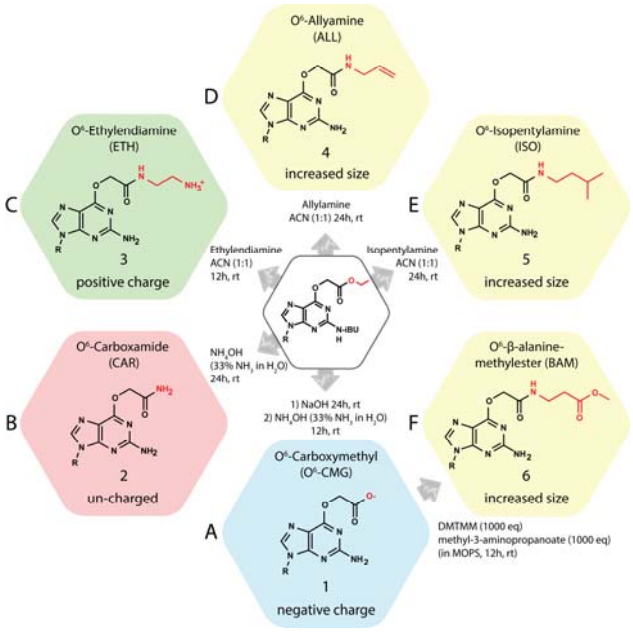

Figure 1. O^6-CMG modifications used for the SAR study. O^6-CMG **(A)** and the analogs CAR, ETH, ALL, and ISO **(B-E)** were obtained via post-synthetic modification of the carboxyethylester; different adducts could be obtained depending on whether NaOH, NH_4OH or primary amines were used. BAM was obtained from O^6-CMG via activation of the carboxylic group with DMTMM followed by coupling with methyl-3-aminopropanoate. R = DNA.

The chemical determinants defining the fidelity of DNA Pols vary[27-31] and there exists a complex interplay of interactions between the Pol, the DNA and the damaged base.[32] Pols η, ι, and κ are characterized by a preformed active site, tailored to accommodate DNA adducts and make functional contacts with the DNA template and the incoming dNTP.[33, 34] These Pols usually poorly overcome or extend from non-hydrogen bonding nucleobases and largely depend on Watson-Crick hydrogen bonding for faithful and efficient DNA synthesis.[29-31, 35] The previous O^6-CMG bypass studies with isolated Pols revealed specific dNTP incorporation patterns opposite O^6-CMG. However, it is unclear how the adduct structure determines the fidelity of Pol η, ι, and κ and in particular what interactions confer the error-free bypass observed by Pol κ.[26]

To address how changes in size and charge of the O^6-CMG adduct impact Pol bypass and contribute to mutations, we performed structure activity profiling studies. We prepared six different DNA templates with minimally altered O^6-CMG structures (Figure 1, A-F) by coupling primary amines to the carboxylic acid group of a site-specific O^6-CMG at codon 12 in the *KRAS* sequence. Standing-start primer extension assays were carried out with the Y-family Pols η, ι, and κ and the X-family Pol β. Further analysis into relevant hydrogen-bonding interactions during the bypass of modified structures, potentially contributing to error-prone or error-free bypass of TLS Pols, was obtained by computational modeling. Understanding mechanisms that define the fidelity of TLS Pols as well as how adduct structure dictates dNTP selection will advance our capacity to predict mutagenicity on the basis of chemical structures.

RESULTS AND DISCUSSION

Preparation of carboxymethyl adduct analogs. O^6-CMG was prepared by a recently reported copper-catalyzed alkylation with diazo compounds, allowing us to chemoselectively introduce a carboxyethylester moiety at the O^6-position of guanosine.[36] The modified nucleoside was incorporated into oligonucleotides via standard phosphoramidite chemistry and subsequently deprotected as previously described[37] to obtain an O^6-CMG modified DNA template (Figure 1, A). To probe the structural determinants of the O^6-CMG bypass, we synthesized carboxymethyl adducts with variations in size and charge post-synthetically by two different strategies via an alkoxide replacement or peptide coupling reaction.

The alkoxide replacement reaction was carried out on oligonucleotides with dmf-dG, Ac-dC, Bz-dA and iBu-dCMG protected nucleobases, which were treated with NH_4OH or the primary amines isopentylamine, ethylenediamine or allylamine. The basicity/nucleophilicity of NH_4OH or the corresponding primary amines led to the removal of all protecting groups from the nucleobases or the phosphate backbone and replaced the alkoxide of the O^6-carboxyethylester with NH_3 or the corresponding primary amine (Figure 1, B-E). Oligonucleotides with modifications 2–5 (Figure 1) were obtained in yields between 50-80%. But, we observed the formation of a side product that was 13 Da higher in mass than the theoretically calculated mass for either the ISO, ETH, or ALL modified oligonucleotide. We were unable to verify the adduct's chemical identity, but attributed the occurrence of the second species to the N^2-isobutyryl (iBu) protecting group because in a test reaction with an N^2-dimethylformamide (dmf) protected O^6-carboxyethylesterguanine (in the DNA template) we did not detect the formation of the side-product.

The second strategy used to prepare the β-alanine-methylester modified adduct involved a DMTMM-mediated activation of the carboxylic acid of the deprotected O^6-CMG template followed by an amide coupling reaction (Figure 1, F). Coupling of the β-alanine-methylester to the carboxylic acid resulted in the desired O^6-β-alanine-methylester modified oligonucleotide (6) in 40-50% yield. We also tested the DMTMM-mediated (4-(4,6-Dimethoxy-1,3,5-triazin-2-yl)-4-methylmorpholinium chloride) amine cou-

pling with ethylenediamine, isopentylamine, and allylamine which gave comparable yields as observed for the β-alanine-methylester reaction.

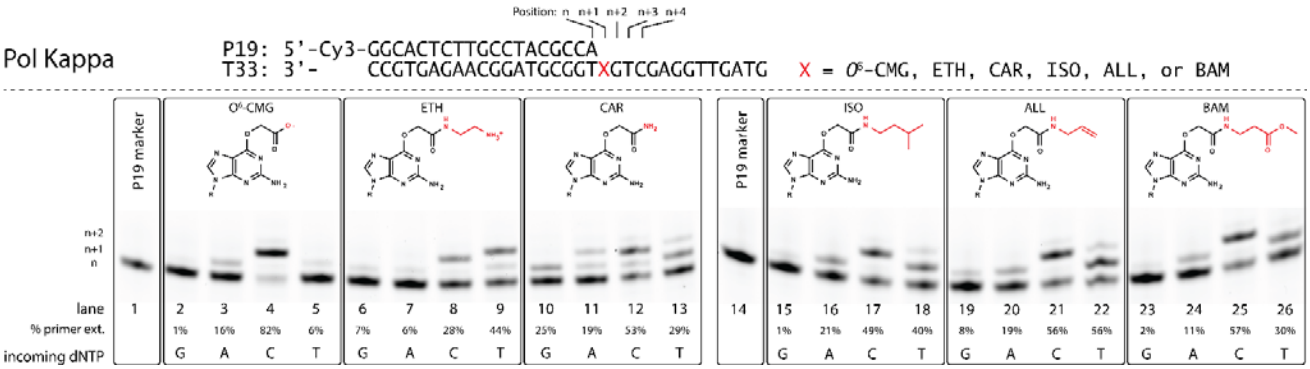

Figure 2. Polymerase extension products observed from Pol κ in the bypass of *O*6-CMG and the synthetic carboxymethyl adducts ETH, CAR, ISO, ALL, and BAM.

In total, we prepared 6 different DNA templates containing *O*6-CMG or an analog with altered sized and charge characteristics (Figure 1). *O*6-CMG (Figure 1, A) is negatively charged under physiological conditions whereas its *O*6-carboxamide (CAR) analog (Figure 1, B) is similar in size (based on surface volume calculations, Table S1) but is neutral. A positive charge was introduced by positioning an amine away from the carbonyl (ETH), (Figure 1, C). ETH is expected to be protonated under physiological conditions, however, it is larger than CMG. Thus, to assess potential effects related to the adduct size, we prepared *O*6-allylamine (ALL), which mimics the size of ETH (Table S1) but is uncharged, whereas *O*6-isopentylamine (ISO) and *O*6-β-alanine-methylester (BAM) (Figure 1, D-F) contain long alkyl chains used to probe steric interactions in the Pol active site.

Pol κ bypasses *O*6-CMG specifically but structural alterations reduce the efficiency and influence the fidelity of the Pol. The ability of Pol κ to bypass *O*6-CMG and the five carboxymethyl analogs was evaluated by primer extension analysis (Figure 2). Pol κ inserted almost exclusively dCMP opposite *O*6-CMG which was displayed by a prominent n+2 band (82%, Figure 2, lane 4). Interestingly, this stringent insertion pattern was unique to *O*6-CMG and Pol κ was more promiscuous for the other five carboxymethyl adducts. We observed that minor alterations of the *O*6-CMG structure, *e.g.* changing the carboxylate group of *O*6-CMG to a carboxamide group (CAR), led to insertion of all four dNMPs (Figure 2, lanes 10-13). The volumes of the modifications at the *O*6-position for *O*6-CMG and CAR are almost identical (e.g. 51 Å3 and 58 Å3 , respectively, Table S1), hence the change in the bypass fidelity of CAR might be attributed to the change of the functional group (COO- to CONH2) rather than to the minimally increased size of the adduct. The apolar and sterically larger adducts ALL, BAM, and ISO also reduced the fidelity of Pol κ but there was little difference in the observed primer extension pattern between ISO, ALL, and BAM (Figure 2, lanes 15-26). Indeed, the similar mutagenic bypass observed for the small CAR as well as for the larger ALL, BAM, and ISO adducts suggested that steric effects do not account for the differences in the Pol fidelity. Due to the charge of *O*6-CMG, we were therefore particularly interested if electrostatic changes may affect the fidelity of Pol κ.

To investigate this hypothesis, we used the ETH analog which is positively charged under physiological conditions due to the ammonium moiety. The volume of the ETH modification (108 Å3) is about twice that of CAR (58 Å3) and the same as ALL (100 Å3). The primer extension data revealed that Pol κ incorporated dTMP and dCMP opposite ETH. It was therefore bypassed with higher fidelity as CAR or ALL but with lower fideltiy than *O*6-CMG. Interestingly, the bypass of ETH was characterized by preferential incorporation of dTMP (44%) over dCMP (28%) (Figure 2, lane 9 and 8). This result was unique, since the bypass of ETH was the only instance amongst all tested adducts where incorporation of dTMP seemed to be preferred over dCMP (Figure S18, A).

To quantitatively assess the misinsertion frequency of Pol κ, we determined steady-state kinetic rates for the negatively charged *O*6-CMG adduct, the neutral CAR analog (identical in size to *O*6-CMG), as well as for the positively charged ETH analog and the uncharged ALL analog (identical in size to ETH). Kinetic parameters K_M and k_{cat} were determined under enzyme-limiting conditions with at least a 10-fold excess of DNA and varying dCTP and dTTP concentrations. Amongst the four DNA substrates tested, Pol κ most efficiently incorporated dCMP opposite CAR with a k_{cat}/K_M of 0.65 $\mu M^{-1}min^{-1}$ (Table 1, entry 2), which was 11-fold more efficient than incorporation of dCMP opposite *O*6-CMG. A large contribution of the efficient Pol κ catalysis opposite CAR seems to derive from the favorable K_M of 1.3 μM, which was the lowest K_M observed. However, incorporation of dCMP opposite *O*6-CMG (k_{cat}/K_M of 0.06 $\mu M^{-1}min^{-1}$, table 1, entry 1) was 17- and 20-fold more efficient than opposite ALL and ETH respectively (Tabel 1, entries 3 and 4).

Interestingly, Pol κ incorporated dTMP opposite ETH with an almost identical k_{cat}/K_M (0.07 $\mu M^{-1}min^{-1}$, Table 1, entry 8) as observed for the incorporation of dCMP opposite *O*6-CMG. Therefore, dTMP incorporation was 23-fold more efficient than incorporation of dCMP opposite ETH. No such drastic difference was observed between the incorporation of dCMP and dTMP opposite ALL (k_{cat}/K_M of 0.004 $\mu M^{-1}min^{-1}$ and 0.003 $\mu M^{-1}min^{-1}$, respectively, Table 1,

entries 3 and 7) which is almost identical in size to ETH. Thus, the change in nucleotide insertion fidelity between ETH and ALL might be a direct effect of the positive charge of ETH. Noteworthy, the K_M as well as the turnover number (k_{cat}) were almost identical between dCMP insertion opposite O^6-CMG (k_{cat} 2.9 min^{-1}) and dTMP insertion opposite ETH (k_{cat} 3.4 min^{-1}) and the highest turnover numbers observed amongst all the analogs tested.

Table 1. Steady-state kinetic analysis for the insertion of dCTP or dTTP on templates containing O^6-CMG, CAR, ETH, and ALL

Pol	Incoming dNTP	Entry	Template	k_{cat} [min^{-1}]	K_M [μM]	k_{cat}/K_M [$\mu M^{-1}min^{-1}$]	fold change
Kappa (κ)	dCTP	1	O^6-CMG	2.9 ± 0.25	47 ± 10	0.06 ± 0.014	1
		2	CAR	0.82 ± 0.021	1.3 ± 0.23	0.65 ± 0.120	+ 11
		3	ALL	0.66 ± 0.077	181 ± 40	0.004 ± 0.0010	- 17
		4	ETH	0.40 ± 0.033	131 ± 27	0.003 ± 0.0010	- 20
	dTTP	5	O^6-CMG	n.d.	n.d.	n.d.	n.d.
		6	CAR	0.16 ± 0.010	15 ± 3.2	0.010 ± 0.0020	- 6
		7	ALL	0.42 ± 0.033	124 ± 22	0.003 ± 0.0010	- 18
		8	ETH	3.4 ± 0.18	49 ± 7.6	0.070 ± 0.010	+ 1.1
Eta (η)	dCTP	9	O^6-CMG	0.13 ± 0.004	20 ± 3.0	0.0065 ± 0.0010	1
		10	CAR	0.10 ± 0.003	8.3 ± 1.4	0.012 ± 0.0020	+ 1.8
		11	ALL	0.15 ± 0.006	61 ± 10	0.0024 ± 0.0010	- 2.7
		12	ETH	0.060 ± 0.002	18 ± 2.4	0.0035 ± 0.0010	- 1.9
	dTTP	13	O^6-CMG	0.090 ± 0.004	22 ± 4.2	0.004 ± 0.0010	- 1.6
		14	CAR	0.050 ± 0.002	6.8 ± 1.2	0.008 ± 0.0010	+ 1.2
		15	ALL	0.10 ± 0.004	8.1 ± 1.4	0.012 ± 0.0020	+ 1.9
		16	ETH	0.19 ± 0.004	2.4 ± 0.40	0.080 ± 0.014	+ 12

These results are partially in line with previous findings where Pol κ preferentially incorporated dCMP over dTMP when bypassing other O^6-alkylguanine adducts such as O^6-MeG, O^6-benzylguanine (O^6-BnG), and O^6-[4-(3-pyridyl)-4-oxobutyl]guanine (O^6-PobG). The increasing steric size of the adducts (O^6-MeG < O^6-BnG < O^6-PobG) reduced the incorporation of dCMP and dTMP but promoted incorporation of dGMP opposite O^6-PobG.[38] In our study, dCMP insertion by Pol κ was preferred over dTMP incorporation for O^6-CMG, CAR, and ALL but not for ETH (Figure S18, A). The increasing size of the adducts had an impact on the efficiency of Pol κ but did not drastically affect the fidelity (dCTP > dTTP) with the exception of ETH which was more efficiently bypassed by insertion of dTMP by Pol κ.

The adduct size of the O^6-CMG analogs enhances the mutagenicity of Pol η. To investigate the tolerance of the Pols to the O^6-CMG adducts in more detail and compare the substrate specificity of Pol κ with other Pols involved in DNA damage bypass, we performed primer extension assays with Pol ι and η as well as with the X-family Pol β. The substrate specificity of all three Pols was less distinct as compared to Pol κ. Amongst all Pols tested, Pol η was the most mutagenic in the bypass of all carboxymethyl adducts. The observed primer extension patterns did not show much variation for all adducts tested and high primer extension percentages for incorporation of dAMP and dTMP opposite all carboxymethyl adducts were observed (Figure S13).

The mutagenic bypass of O^6-CMG was previously kinetically characterized by predominant insertion of dAMP[26] which was unique, compared with the other O^6-alkylG adducts i.e. O^6-MeG, O^6-BnG, O^6-PobG.[38] The differences in the structures of O^6-MeG, O^6-BnG, O^6-PobG and O^6-CMG, together with the similarities in the Pol η primer extension patterns observed for the tested carboxymethyl adducts in this study, suggest that the preference for dAMP insertion of Pol η opposite O^6-CMG is likely a consequence of interactions with the CO itself rather than with atoms bonded to it and potential steric or charge-charge interactions with them.

To identify differences in the adduct bypass of Pol κ and Pol η in a quantitative way, we also determined steady-state kinetic rates for the bypass of O^6-CMG, CAR, All and ETH by Pol η. Interestingly, Pol η most efficiently incorporated dTMP opposite ETH (k_{cat}/K_M of 0.080 $\mu M^{-1}min^{-1}$, Table 1, entry 16) and did so 23-fold more efficient as for incorporation of dCMP opposite ETH (k_{cat}/K_M of 0.0035 $\mu M^{-1}min^{-1}$, Table 1, entry 12). In contrary to the high k_{cat} observed for insertion of dTMP opposite ETH by Pol κ, the increased efficiency can be attributed to a favorable K_M of 2.4 μM, which was the most favorable observed for all Pol η kinetic parameters. In addition, Pol η preferred incorporation of dCMP over dTMP only for the small O^6-CMG and CAR analogs (k_{cat}/K_M of 0.0065 $\mu M^{-1}min^{-1}$ and 0.012 $\mu M^{-1}min^{-1}$, respectively, Table 1, entries 9 and 10) and a decreased dCMP incorporation-efficiency was observed for the bulkier ALL and ETH analogs (k_{cat}/K_M of 0.0024 $\mu M^{-1}min^{-1}$ and 0.035 $\mu M^{-1}min^{-1}$, respectively, Table 1, entries 11 and 12).

Previous kinetic studies demonstrated that the bypass of Pol η past O^6-alkylG adducts was dominated by incorporation of dCMP and dTMP opposite the smaller O^6-MeG and O^6-BnG adducts,[38] similar to our observation for the bypass of O^6-CMG and CAR (Figure S18, B). However, for the larger O^6-PobG adduct, dTMP incorporation-efficiency decreased and more dGMP insertion was observed.[38] Here, our kinetic experiments revealed that the larger ETH and ALL analogs were more efficiently bypassed by dTMP and the dCMP incorporation-efficiency was decreased (Figure S18, B). Thus, the increased steric size of ALL and ETH might contribute to a more efficient mutagenic bypass of Pol η and leading to an increased incorporation of dTMP, whereas the smaller O^6-CMG and CAR analogs favored incorporation of dCMP (Figure S18, B).

In addition, the processivity of Pol ι was similar to Pol κ but we didn't observe sensitive towards a specific adduct. For all tested adducts the insertion of dTMP was preferred over dCMP whereas only little incorporation of dAMP and no incorporation of dGMP was observed (Figure S14). The preference for dTMP insertion by Pol ι is probably due to the architecture of the Pol active site and the induction of a template purines to adopt a *syn* conformation, which causes a Hoogsteen base pair with an incoming dTTP.[39] The same pattern was found for Pol β, which is involved in base excision repair (BER) (Figure S15).

In summary, Pol κ, ι, η, and β were effective in the bypass of O^6-CMG and the structure variations of the carboxymethyl adducts seem to influence the fidelity of Pol κ. Moreover, the increased steric size of ALL and ETH decreased that fidelity of Pol η, whereas the dNTP preference of the other Pols is not affected. Nonetheless, it remained unclear what interactions between the Pol and the DNA or the incoming dNTP are responsible for this difference in dNTP selection.

Computational modeling suggests a role for interbase hydrogen bonding for error-free bypass of O^6-CMG by Pol κ. The primer extension assays revealed that Pol κ is specific in the bypass of O^6-CMG, however, every variation of the O^6-CMG structure (tested in this study) resulted in a more mutagenic bypass of the adducts by the Pol. In the absence of any structural data for O^6-CMG we decided to use computational modeling to rationalize our findings and to understand how differences in the adduct structures influence Pol κ fidelity. Replicative Pols often use a combination of geometric fit and shape complementarity to discriminate matched- from mismatched base pairs. In contrast, Y-family Pols cannot use a conformation-induced selection mechanism due to their large and solvent exposed active site. Instead, there is evidence that the TLS Pols κ, η, and Dpo4 employ hydrogen bonding to select the correct nucleotide.[30, 40-42] Therefore, the specific bypass of O^6-CMG by Pol κ could be directly related to an energetically more favorable hydrogen bonding pattern between O^6-CMG and dCTP as compared to dTTP, dGTP and dATP.

Our modeling approach focused on identifying differences in the interbase hydrogen bonding pattern between the templating base and the incoming nucleotide. A ternary crystal structure of Pol κ (PDB: 5W2A)[43] in complex with a primer-template strand and an incoming dCTP was modeled with Molecular Operating Environment (MOE) software. All modified structures were prepared with the MOE QuickPrep functionality and energy minimized with the Amber 99 force field.

To investigate the molecular basis for the specific- and error-free bypass of O^6-CMG by Pol κ, we compared computational models of O^6-CMG:dCTP, O^6-CMG:dTTP, O^6-CMG:dATP and O^6-CMG:dGTP (Figure 3, B-E) in the Pol κ active site. The O^6-CMG:dCTP base pair (Figure 3, B) adopts a coplanar wobble base pair with three hydrogen bonds between the N^1, the N^2 and the carboxylate residue of O^6-CMG with the pairing dCTP. The O^6-CMG:dTTP base pair forms two hydrogen bonds in a Watson-Crick-geometry but the potential repulsion between the O^6 of CMG and the O^4 of dTTP prevents optimal alignment and moves the incoming dTTP out of plane relative to the templating base (Figure 3, C). O^6-CMG:dATP as well as O^6-CMG:dGTP can both form hydrogen bonds with the carboxylate residue of O^6-CMG, however, both dNTPs are displaced in the active site and out of plane relative to O^6-CMG (Figure 3, D + E). We found that the dCTP:O^6-CMG pair formed the most dense hydrogen bonding pattern, while being in a coplanar geometry; whereas dTTP and in particular dATP and dGTP were misaligned in the Pol active site. Hydrogen bonding, base pair geometry and also the base stacking are important factors that directly contribute to the polymerase fidelity[44, 45] and might be responsible for the specific bypass of O^6-CMG by Pol κ.

Support for the importance of the base pair geometry and hydrogen bonding for the fidelity of Pol κ can be derived from previous research with *Sulfolobus solfataricus* DNA polymerase Dpo4 (an archaeal homolog of Pol κ). Dpo4-catalzyed primer extension products demonstrated that O^6-MeG was bypassed mainly by insertion of dCTP and only to a minor extent by dTTP.[46] A crystal structure for dCTP paired opposite O^6-MeG in the active site of Dpo4 revealed that the bypass proceeds by pairing dCMP in a wobble geometry with the O^6-MeG, forming two hydrogen bonds.[46] In contrast, structural data for dTTP paired opposite O^6-MeG in the same enzyme displayed disordered base pairing, potentially in a pseudo-Watson-Crick geometry.

In total three possible O^6-MeG:dTTP structures were predicted, thus indicating that there is not one which is strongly energetically favoured.[46] Noteworthy, the same base pairing modes were detected crystallographicaly for the bulky adduct O^6-benzylguanine (O^6-BnG) in the active site of Dpo4,[47] in agreement with the base pairing patterns observed in the models herein (Figure 3, B + C). Similar to Dpo4, the O^6-CMG:dCTP wobble base pair, modeled in the Pol κ active site, might be energetically more favored due to the three hydrogen bonds as compared to the pseudo-Watson-Crick O^6-CMG:dTTP base pair.

Polymerase bypass of the ETH adduct by Pol κ was less specific as compared to O^6-CMG but not as mutagenic as for the other four O^6-CMG adducts. In order to identify differences in hydrogen bonding, potentially responsible for the altered dNTP selectivity we thought to model ETH paired with an incoming dNTP in the Pol κ active site and compare these models to O^6-CMG-structures.

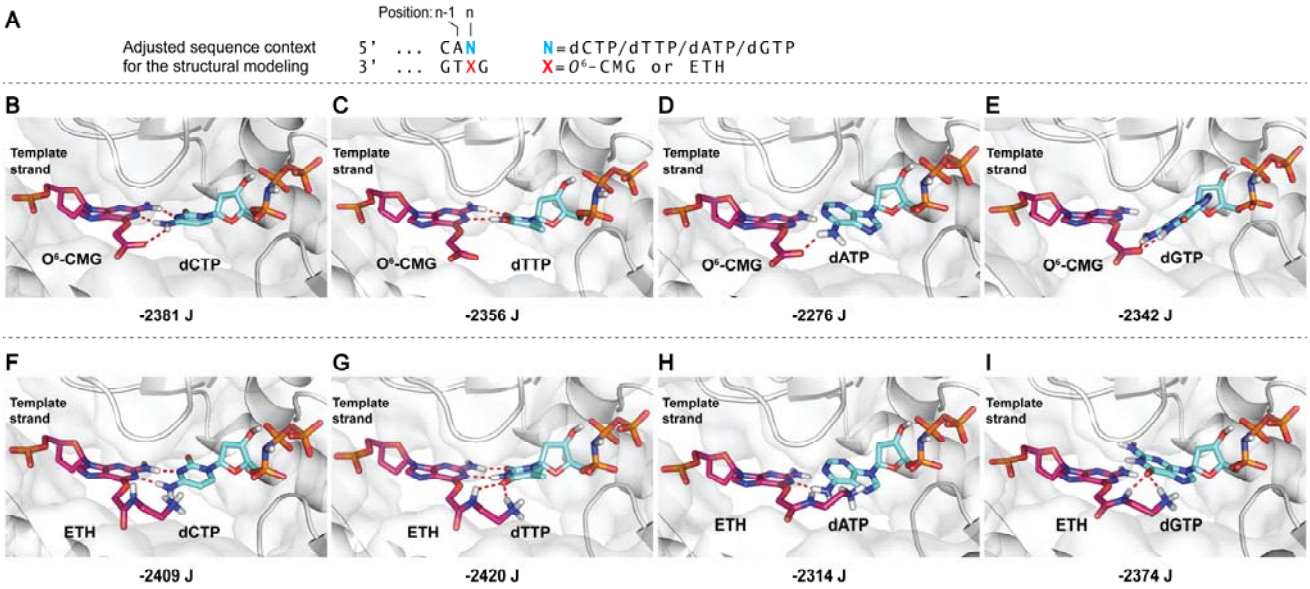

Figure 3. Computational modeling of O^6-CMG or ETH in the Pol κ active site. **(A)** Adjusted sequence context with X = O^6-CMG or ETH and N = the incoming dNTP. Structural models of (**B**) O^6-CMG:dCTP, (**C**) O^6-CMG:dTTP, (**D**) O^6-CMG:dATP, and (**E**) O^6-CMG:dGTP. (**G**) Structural model of (**F**) ETH:dCTP, (**G**) ETH:dTTP, (**H**) ETH:dATP, and (**I**) ETH:dGTP. The numbers below each modeled structure represent the minimized potential energy (J) of the corresponding base pair.

The model of the ETH:dCTP base pair suggested a coplanar wobble-geometry and forms two hydrogen bonds between the N^1 and N^2 of ETH and dCTP (Figure 3, F). ETH:dTTP adopts a coplanar Watson-Crick base-pair geometry with two hydrogen bonds emanating from N^1 and N^2 of ETH and the other two from the amine and ammonium residue (Figure 3, G). The computational model of ETH:dATP displayed one hydrogen bond between the N^1 of ETH and the N^6 of dATP (Figure 3, H), whereas the model for ETH:dGTP predicted two hydrogen bonds between the amine and ammonium residue of ETH and the O^6 of dGTP. In addition, dATP and also dGTP were moved out of plane relative to the templating ETH, thereby adopting an unfavorable geometry within the active site. The observed base pairing geometries for ETH were very similar to the modeled O^6-CMG base pairs however, with particular differences in the hydrogen bonding patterns. The incoming dTTP is better stabilized upon pairing with ETH due to two additional hydrogen bonds whereas dCTP forms only two hydrogen bonds with ETH (Figure 3, F and G). The better stabilization of ETH:dTTP in comparison to ETH:dCTP, may serve as an explanation for the preferred incorporation of dTMP and is supported by the low potential energy (e.g. -2420 J, Figure 3, G) predicted by modeling.

In order to assess the importance for hydrogen-bonding suggested by the above model, we performed primer extension experiments with modified nucleosides zebularine (dZEB), closely resembling C but lacks the 4'-amino group, and dihydropyrimido[4,5-c][1,2]oxazin-7-one (dPTP), which has two tautomeric forms and can hydrogen bond similar to C or T but is larger (Figure S19, C). Modeling the incoming dZEB in the Pol κ active site revealed that dZEB forms only one hydrogen bond with O^6-CMG as well as with ETH (Figure S20, B and D), and the primer extension assays revealed that dZEB was neither incorporated opposite O^6-CMG nor opposite ETH (Figure S19, A and B). This observation further supports that hydrogen bonding interactions emanating from the 4'-amino group of dCTP are important for dNTP selectivity by Pol κ and stabilize the positioning of the carboxylate group for high dCTP selectivity by Pol κ (compare Figure 3, B and F and Figure S20 B and D). In contrast to dZEB, the structural modeling of dPTP paired with O^6-CMG and ETH suggested geometries and hydrogen-bonding patterns similar to dTTP and despite its increased size, it was incorporated opposite ETH and to some extent O^6-CMG (Figure S19, A and B). These data reinforce hydrogen bonding stabilization as a basis for nucleotide selection opposite O^6-CMG.

Since the bypass of ETH by Pol κ was also characterized by a strong n+2 primer extension band (Figure 2, lanes 8 and 9), we hypothesized that the ETH adduct might have a stabilizing effect on the subsequent primer extension step. To investigate this possibility, we modeled the ETH:T and the ETH:C base pair in the post-insertion step (Figure S16). The structural model suggested that ETH can stabilize the incoming dTTP as well as the templating G through hydrogen bonds emanating from the ETH ammonium residue. At the same time, ETH maintains three hydrogen bonds with the paired T in a Watson-Crick geometry (Figure S16, B). In contrast, when C is paired with ETH, the ammonium side-chain at the O^6-position of ETH is positioned away from the Watson-Crick face. Thus, it does not interfere with the hydrogen bonding of G and incoming dCTP, but also does not confer any favorable interactions (Figure S16, C).

Since O^6-CMG as well as ETH contain pH sensitive functional groups, we were also curious if changes of the charge state may influence the fidelity of Pol κ. Previous work showed that *E coli*. Pol II and IV benefit from electrostatic effects and are insensitive to steric changes of base pairs.[48] Thus, we adjusted the structure of O^6-CMG or ETH to the

corresponding protonated (COOH for O^6-CMG) or deprotonated state (NH_2 for ETH) in the MOE software and assessed the changes in hydrogen bonding with the incoming dCTP or dTTP by energy-minimization. O^6-$CMG_{(COOH)}$ paired with dCTP lost the hydrogen bond between the carboxylate group and the N^4 of dCTP (Figure S17, B), and $ETH_{(NH_2)}$ paired with dCTP had an additional hydrogen bond (Figure S17, C). In contrast, no changes in the hydrogen bonding pattern for $ETH_{(NH_2)}$:dTTP was observed (Figure S17, D). These models suggested that charges within carboxymethyl adducts can determine nucleotide selection via interaction with the incoming dNTP.

Conclusion. The results obtained from this study demonstrate that Pol κ is specific in the bypass of O^6-CMG but extremely minor changes of the carboxymethyl structure strongly reduce the fidelity of the Pol. In addition, the computational modeling suggest that hydrogen bonding between the templating base and the incoming nucleotide provides a driving force for the selection of the preferred dNTP. Despite the large degree of structural overlap shared amongst the Y-family TLS Pols, Pol η and ι had less bypass selectivity towards a particular carboxymethyl adduct. A unique structural feature of Pol κ is the N-clasp motif on the major groove side, which stabilizes the catalytic complex, and is absent in other Y-family Pols.[49, 50] The modification at the O^6-position are major-groove DNA adducts and possibly interact with the N-clasp motif, which may explain the higher sensitivity of Pol κ towards the structural variations. Therefore, further chemical characterization and computational modeling would be required to delineate the molecular interactions in more detail. In addition, crystal structures of the O^6-CMG adduct in complex with TLS Pols will be crucial for a clear picture of which molecular interactions control the observed polymerase fidelities.

METHODS

Chemical reagents and materials. dNTPs were purchased from Invitrogen (Switzerland) and Bioconcept (Switzerland). dZEB and dPTP were purchased from TriLink Biotechnologies (USA). TRIS-HCl (pH 7.0 at 25°C), TRIS-HCl (pH 8.0 at 25°C), NaCl, $MgCl_2$, dithiothreitol (DTT) and glycerol were all purchased from Invitrogen (Switzerland). Bovine serum albumin (BSA) was obtained from New England Biolabs (Ipswich, MA, USA). Sep-Pak® C18 classic cartridges were purchased from Waters (Milford, MA, USA). All other reagents were purchased from Sigma Aldrich (Switzerland). Pols η, κ, and ι were purchased from Enzymax (Lexington, KY, USA). Pol β was a generous gift from Prof. Samuel Wilson, National Institutes of Environmental Health Sciences (Durham, USA). O^6-CMG phosphoramidite was prepared by adaptation of a previous method.[36] Synthetic details and characterization of nucleoside intermediates are described in supplementary information.

Oligonucleotides. Template sequences were: (33mer), 5'-GTAGTTGGAGCTGXTGGCGTAGGCAAGAGTGCC-3'
where X = G, O^6-CMG, ETH, CAR, ALL, ISO, or BAM. The G-containing strand was ordered HPLC-pure from Eurofins Genomics (Germany). The O^6-CMG (CMG) containing template was synthesized on a Mermade 4 DNA synthesizer from Bio Automation Corporation (Plano, TX) using standard conditions and base-labile phosphoramidites (dmf-dG-CE, Ac-dC-CE, and dA-CE). After DNA synthesis the O^6-carboxymethylester containing 33mer sequence was deprotected as described previously by Millington *et al.*[37] to yield the CMG modification. The synthesis was performed in trityl-on mode and the oligonucleotides were post-synthetically purified on a Sep-Pak® C18 cartridge (www.waters.com) to remove truncated sequences. Elution of the desired oligonucleotide consisted of cleaving the DMT group and collection of the desired DNA. Subsequently the template was purified by reverse phase high-performance liquid chromatography (RP-HPLC) with a linear gradient from 10-13 % (v/v) acetonitrile in 50 mM triethylammonium acetate over 25 min.

Modification of O^6-CMG by ester deprotection. The CAR-containing 33mer oligonucleotide was obtained by deprotection of the O^6-carboxyethylester-containing oligonucleotide with NH_4OH (33% NH_3 in H_2O) at room temperature (RT) for 24 h. The ISO-, ALL- and ETH-containing sequences were obtained by deprotecting the O^6-carboxyethylester-containing oligonucleotide with isopentylamine, allylamine or ethendiamine, respectively, in acetonitrile (1:1) for 24 h at RT. The solution of deprotection reactions of CAR, ISO, ALL, and ETH were evaporated to dryness, re-suspended in 100 mM TEAA buffer and pre-purified with a Sep-Pak® C18 cartridge as described in the oligonucleotide section. All modified templates were subsequently purified by RP-HPLC on a Phenomenex Luna® (5 µm, C18, 100 Å) column with a linear gradients from 11-16 % (ISO and ALL), 10-14 % (ETH), and 10-15 % (CAR) (v/v) acetonitrile in 50 mM triethylammonium acetate over 25 min.

Peptide coupling reaction. The BAM modification was introduced via an amine coupling reaction with the carboxylate group in the O^6-position of O^6-CMG. Coupling reactions were carried out with 1-20 nM of the O^6-CMG-containing 33mer template in MOPS buffer (50 mM, 0.5 M NaCl, pH 8). The carboxylate group was activated with DMTMM (4-(4,6-dimethoxy-1,3,5-triazin-2-yl)-4-methylmorpholinium chloride) (1000 eq) at RT for 45 min on a Thermo-Shaker (1000 rpm). Then methyl-3-aminopropanoate (1000 eq) was added and the reaction was kept on the Thermo-Shaker overnight (rt, 500 rpm). Subsequently, the DNA was isolated via ethanol precipitation and purified by RP-HPLC on a Phenomenex Luna® (5 µm, C18, 100 Å) column with a linear gradient from 10-14 % (v/v) acetonitrile in 50 mM triethylammonium acetate over 25 min.

DNA primer strand. The sequence for the Cy3-labeled oligonucleotide primer strands was as follows: (19mer) 5'-Cy3-GGCACTCTTGCCTACGCCA-3'. The primer was purchased from Eurofins Genomics (Germany) and purified purified by polyacrylamide gel electrophoresis (PAGE). The presence of all desired DNA products was confirmed by mass spectrometry (supporting information) performed on an Agilent MSD ion trap mass spectrometer with electrospray ionization, operated in negative ion mode. The concentration was determined by UV spectroscopy at 260 nm on a NanoDrop 1000.

Primer extension assays. A Cy3-labeled primer was annealed to a complementary 33mer template (5'-GTAGTTGGAGCTGXTGGCGTAGGCAAGAGTGCC-3' with X = O^6-CMG, CAR, ISO, ALL, ETH, or BAM). The annealing reactions were carried out by heating at 95 °C for five minutes and allowing to cool to RT for 3 h. The primer extension reactions were carried out in a reaction buffer containing 40 mM Tris-HCl (pH 8.0, 25 °C), 1 mM $MgCl_2$, 10 mM DTT, 250 μg/ml BSA and 3% glycerol. Further, 200 nM 5'-Cy3-primer-template DNA and 40 nM of the polymerase were used. The reaction was started by addition of 100 μM dATP, dGTP, dCTP, dTTP, 10 μM, 50 μM or 100 μM dZEB or dPTP, to the sample containing the buffer, 5'-Cy3-primer-template DNA and the Pol. The reaction mixture was incubated for 25 min at 37 °C and the reaction was terminated by adding 10 μL of quenching solution (80 % formamide with 10 mM NaOH, 0.1 M EDTA and a trace of bromophenol blue and xylene cyanol). The resulting solution was loaded on a 15 % polyacrylamide 7 M urea gel, run for 2.5 hours at 550 V and visualized with a ChemiDoc Imager (BioRad, Hercules, CA).

Steady-state kinetics. Steady-state kinetics were performed with Pol κ and η under a range of dCTP and dTTP concentrations. A Cy3-labeled primer was annealed to the complementary template for the primer extension assays, which contained O^6-CMG, CAR, ETH, or ALL. For the enzymatic reactions, 5 nM of Pol κ or 10 nM or Pol η were allowed to react with 100 nM 5'-Cy3-primer-template DNA at 37 °C in reaction buffer containing 40 mM Tris-HCl (pH 8.0 at 25 °C), 1 mM $MgCl_2$, 5 mM DTT, 250 μg/mL BSA, and 3 % glycerol. All reactions were perofrmed three times. Reactions were quenched at veraious time points with stop dye (80 % formamide with 10 mM NaOH, 0.1 M EDTA and a trace of bromophenol blue and xylene cyanol). The aliquots were loaded on a 15 % polyacrylamide 7 M urea gel and separated by electrophoresis (500 V , 2.5 h). The product bands were analyzed with a ChemiDoc Imager and quantified with ImageLab 5 software (BioRad Hercules, CA). The nucleotide incorporation rate (v_{obs}) was plotted as a function of the dCTP or dTTP concentration and fit into a rectangular hyperbola using the Michaelis-Menten equation to obtain K_M and V_{max}. The k_{cat} was obtained by dividing V_{max} by the total enzyme concentration.

***In silico* modeling experiments.** Model structures were computed with Molecular Operating Environment (MOE) software suite (Chemical Computing Group Inc., Montreal, QC, Canada). A tertiary crystal structure of Pol κ (PDB: 5W2A) was used for the modeling experiments with incoming ddCTP, a 13 mer template (5'-ATGXCTGATCCGC-3' with X= lucidin-N2-G) and a 9mer primer (5'-GCGGATCAG-3') was used for all modeling experiments. The crystal structures was modified with the MOE builder tool, to match the sequence context in our *in vitro* assays. The template was changed to 5'-ATGX**TG**GATCCGC-3' with X = O^6-CMG or ETH and the primer to 5'-GCGGATC**CA**-3'. The polymerase structure was prepared with the MOE QuickPrep function with default settings, including corrections of structural errors, addition of hydrogens, 3D optimization of H-bonding networks and deletion of water molecules further than 4.5 Å from the protein, and restrained minimization within 8 Å from the modified base pairs. For energy minimization, the Amber99 force field was used. Graphical visualization of results was performed in PyMol software (Schrödinger, New York).

ASSOCIATED CONTENT

Supporting Information. Synthesis details, characterization of nucleoside intermediates, HPLC traces, mass spectrometry analysis of O^6-CMG and carboxymethyl adduct-containing DNA and primer extension pictures are described in the supporting information. This material is available free of charge via the Internet at http://pubs.acs.org.

AUTHOR INFORMATION

Corresponding Author

*To whom correspondence should be addressed: Shana J. Sturla, Email: sturlas@ethz.ch

Notes

The authors declare no competing financial interest

ACKNOWLEDGMENT

We thank Dnyaneshwar Rasale and Seemon Coomar for help with the preparation of the O^6-CMG nucleoside and Prof. Dr. Dario Neri, Gabriele Bassi and Cedric Stress for helpful input regarding the peptide coupling reaction. This work was supported by the Swiss National Science Foundation (156280).

REFERENCES

1. Friedberg, E. C., McDaniel, L. D., and Schultz, R. A. (2004) The role of endogenous and exogenous DNA damage and mutagenesis, *Curr. Opin. Genet. Dev. 14*, 5-10.
2. Mirvish, S. S. (1995) Role of N-nitroso compounds (NOC) and N-nitrosation in etiology of gastric, esophageal, nasopharyngeal and bladder cancer and contribution to cancer of known exposures to NOC, *Cancer Lett. 93*, 17-48.
3. Fahrer, J., and Kaina, B. (2013) O6-methylguanine-DNA methyltransferase in the defense against N-nitroso compounds and colorectal cancer, *Carcinogenesis 34*, 2435-2442.
4. Tricker, A. R., and Preussmann, R. (1991) Carcinogenic N-nitrosamines in the diet: occurrence, formation, mechanisms and carcinogenic potential, *Mutat. Res. 259*, 277-289.
5. Drablos, F., Feyzi, E., Aas, P. A., Vaagbo, C. B., Kavli, B., Bratlie, M. S., Pena-Diaz, J., Otterlei, M., Slupphaug, G., and Krokan, H. E. (2004) Alkylation damage in DNA and RNA--repair mechanisms and medical significance, *DNA repair 3*, 1389-1407.
6. Fu, D., Calvo, J. A., and Samson, L. D. (2012) Balancing repair and tolerance of DNA damage caused by alkylating agents, *Nat. Rev. Cancer. 12*, 104-120.
7. Shuker, D. E. G., and Margison, G. P. (1997) Nitrosated Glycine Derivatives as a Potential Source of O^6-Methylguanine in DNA, *Cancer Res.*, 366-369.
8. Lundberg, J. O., and Weitzberg, E. (2013) Biology of nitrogen oxides in the gastrointestinal tract, *Gut 62*, 616-629.
9. Gates, K. S. (2009) An overview of chemical processes that damage cellular DNA: spontaneous hydrolysis, alkylation,

and reactions with radicals, *Chem. Res. Toxicol. 22*, 1747-1760.
10. Mitra, G., Pauly, G. T., Kumar, R., Pei, G. K., Hughes, S. H., Moschel, R. C., and Barbacid, M. (1989) Molecular analysis of O6-substituted guanine-induced mutagenesis of ras oncogenes, *Proc. Natl. Acad. Sci. 86*, 8650-8654.
11. Pauly, G. T., and Moschel, R. C. (2001) Mutagenesis by O6-methyl-, O6-ethyl, and O6-benzylguanine and O4-methylguanine in human cells: effects of O6-alkylguanine-DNA transferease and mismatch repair, *Chem. Res. Toxicol. 14*, 594-900.
12. Fearon, E. R. (2011) Molecular genetics of colorectal cancer, *Annu. Rev. Pathol. 6*, 479-507.
13. Armaghany, T., Wilson, J. D., Chu, Q., and Mills, G. (2012) Genetic alterations in colorectal cancer, *Gastrointest. Cancer. Res. 5*, 19-27.
14. See, K. Y., Jelinsky, S. A., and Loechler, E. L. (2000) Factors that influence the mutagenic patterns of DNA adducts from chemical carcinogens, *Mutat. Res., Rev. Mutat. Res. 463*, 215-246.
15. Prior, I. A., Lewis, P. D., and Mattos, C. (2012) A comprehensive survey of Ras mutations in cancer, *Cancer Res. 72*, 2457-2467.
16. Burns, P. A., Gordon, A. J., and Glickman, B. W. (1988) Mutational specificity of N-methyl-N-nitrosourea in the lacI gene of Escherichia coli, *Carcinogenesis 9*, 1607-1610.
17. Gottschalg, E., Scott, G. B., Burns, P. A., and Shuker, D. E. (2007) Potassium diazoacetate-induced p53 mutations in vitro in relation to formation of O6-carboxymethyl- and O6-methyl-2'-deoxyguanosine DNA adducts: relevance for gastrointestinal cancer, *Carcinogenesis 28*, 356-362.
18. Cupid, B. C., Zeng, Z., Singh, R., and Shuker, D. E. (2004) Detection of O6-carboxymethyl-2'-deoxyguanosine in DNA following reaction of nitric oxide with glycine and in human blood DNA using a quantitative immunoslot blot assay, *Chem. Res. Toxicol. 17*, 294-300.
19. Lewin, M. H., Bailey, N., Bandaletova, T., Bowman, R., Cross, A. J., Pollock, J., Shuker, D. E., and Bingham, S. A. (2006) Red meat enhances the colonic formation of the DNA adduct O6-carboxymethyl guanine: implications for colorectal cancer risk, *Cancer Res. 66*, 1859-1865.
20. Povey, A. C., Hall, C. N., Badawi, A. F., Cooper, D. P., and O'Connor, P. J. (2000) Elevated levels of the pro-carcinogenic adduct, O6-methylguanine, in normal DNA from the cancer prone regions of the large bowel, *Gut 47*, 362-365.
21. Hall, C. N., Badawi, A. F., O'Connor, P. J., and Saffhill, R. (1991) The detection of alklylation damage in the DNA of human gastrointestinal tissues, *Br. J. Cancer 64*, 59-63.
22. Bingham, S. A., Pignatelli, B., Pollock, J. R., Ellul, A., Malaveille, C., Gross, G., Runswick, S., Cummings, J. H., and O'Neill, I. K. (1996) Does increased endogenous formation of N-nitroso compounds in the human colon explain the association between red meat and colon cancer?, *Carcinogenesis 17*, 515-523.
23. Ochs, S., and Severin, T. (1994) Reaction of 2′-Deoxyguanosine with Glyceraldehyde, *Liebigs Ann. Chem. 1994*, 851-853.
24. Schneider, M., Thoss, G., Hubner-Parajsz, C., Kientsch-Engel, R., Stahl, P., and Pischetsrieder, M. (2004) Determination of glycated nucleobases in human urine by a new monoclonal antibody specific for N2-carboxyethyl-2'-deoxyguanosine, *Chem. Res. Toxicol. 17*, 1385-1390.
25. Wu, J., Wang, P., Li, L., Williams, N. L., Ji, D., Zahurancik, W. J., You, C., Wang, J., Suo, Z., and Wang, Y. (2017) Replication studies of carboxymethylated DNA lesions in human cells, *Nucleic Acids Res. 45*, 7276-7284.
26. Raz, M. H., Dexter, H. R., Millington, C. L., van Loon, B., Williams, D. M., and Sturla, S. J. (2016) Bypass of Mutagenic O(6)-Carboxymethylguanine DNA Adducts by Human Y- and B-Family Polymerases, *Chem. Res. Toxicol. 29*, 1493-1503.
27. Morales, J. C., and Kool, E. T. (1998) Efficient replication between non-hydrogen-bonded nucleoside shape analogs, *Nat. Struct. Biol. 5*, 950-954.
28. Morales, J. C., and Kool, E. T. (2000) Varied molecular interactions at the active sites of several DNA polymerases: Nonpolar nucleoside isosteres as probes, *J. Am. Chem. Soc. 122*, 1001-1007.
29. Washington, M. T., Helquist, S. A., Kool, E. T., Prakash, L., and Prakash, S. (2003) Requirement of Watson-Crick hydrogen bonding for DNA synthesis by yeast DNA polymerase eta, *Mol. Cell. Biol. 23*, 5107-5112.
30. Wolfle, W. T., Washington, M. T., Kool, E. T., Spratt, T. E., Helquist, S. A., Prakash, L., and Prakash, S. (2005) Evidence for a Watson-Crick hydrogen bonding requirement in DNA synthesis by human DNA polymerase kappa, *Mol. Cell. Biol. 25*, 7137-7143.
31. Gahlon, H. L., Boby, M. L., and Sturla, S. J. (2014) O6-alkylguanine postlesion DNA synthesis is correct with the right complement of hydrogen bonding, *ACS Chem. Biol. 9*, 2807-2814.
32. Yang, W., and Gao, Y. (2018) Translesion and Repair DNA Polymerases: Diverse Structure and Mechanism, *Annu. Rev. Biochem.*
33. Sale, J. E., Lehmann, A. R., and Woodgate, R. (2012) Y-family DNA polymerases and their role in tolerance of cellular DNA damage, *Nat. Rev. Mol. Cell. Biol. 13*, 141-152.
34. Yang, W. (2014) An overview of Y-Family DNA polymerases and a case study of human DNA polymerase eta, *Biochemistry 53*, 2793-2803.
35. Krueger, A. T., and Kool, E. T. (2007) Model systems for understanding DNA base pairing, *Curr Opin Chem Biol 11*, 588-594.
36. Geigle, S. N., Wyss, L. A., Sturla, S. J., and Gillingham, D. G. (2017) Copper carbenes alkylate guanine chemoselectively through a substrate directed reaction, *Chem. Sci. 8*, 499-506.
37. Millington, C. L., Watson, A. J., Marriott, A. S., Margison, G. P., Povey, A. C., and Williams, D. M. (2012) Convenient and efficient syntheses of oligodeoxyribonucleotides containing O(6)-(carboxymethyl)guanine and O(6)-(4-oxo-4-(3-pyridyl)butyl)guanine, *Nucleosides, Nucleotides Nucleic Acids 31*, 328-338.
38. Choi, J. Y., Chowdhury, G., Zang, H., Angel, K. C., Vu, C. C., Peterson, L. A., and Guengerich, F. P. (2006) Translesion synthesis across O6-alkylguanine DNA adducts by recombinant human DNA polymerases, *J. Biol. Chem. 281*, 38244-38256.
39. Nair, D. T., Johnson, R. E., Prakash, S., Prakash, L., and Aggarwal, A. K. (2004) Replication by human DNA polymerase-iota occurs by Hoogsteen base-pairing, *Nature 430*, 377-380.
40. Washington, M. T., Helquist, S. A., Kool, E. T., Prakash, L., and Prakash, S. (2003) Requirement of Watson-Crick Hydrogen Bonding for DNA Synthesis by Yeast DNA Polymerase η *Mol. Cell. Biol. 23*, 5107-5112.
41. Mizukami, S., Kim, T. W., Helquist, S. A., and Kool, E. T. (2006) Varying DNA base-pair size in subangstrom

increments: evidence for a loose, not large, active site in low-fidelity Dpo4 polymerase, *Biochemistry 45*, 2772-2778.
42. Gahlon, H. L., and Sturla, S. J. (2013) Hydrogen bonding or stacking interactions in differentiating duplex stability in oligonucleotides containing synthetic nucleoside probes for alkylated DNA, *Chemistry 19*, 11062-11067.
43. Yockey, O. P., Jha, V., Ghodke, P. P., Xu, T., Xu, W., Ling, H., Pradeepkumar, P. I., and Zhao, L. (2017) Mechanism of Error-Free DNA Replication Past Lucidin-Derived DNA Damage by Human DNA Polymerase kappa, *Chem. Res. Toxicol. 30*, 2023-2032.
44. Kunkel, T. A. (2004) DNA replication fidelity, *J. Biol. Chem. 279*, 16895-16898.
45. Lee, H. R., Helquist, S. A., Kool, E. T., and Johnson, K. A. (2008) Importance of hydrogen bonding for efficiency and specificity of the human mitochondrial DNA polymerase, *J. Biol. Chem. 283*, 14402-14410.
46. Eoff, R. L., Irimia, A., Egli, M., and Guengerich, F. P. (2007) Sulfolobus solfataricus DNA polymerase Dpo4 is partially inhibited by "wobble" pairing between O6-methylguanine and cytosine, but accurate bypass is preferred, *J. Biol. Chem. 282*, 1456-1467.
47. Eoff, R. L., Angel, K. C., Egli, M., and Guengerich, F. P. (2007) Molecular basis of selectivity of nucleoside triphosphate incorporation opposite O6-benzylguanine by sulfolobus solfataricus DNA polymerase Dpo4: steady-state and pre-steady-state kinetics and x-ray crystallography of correct and incorrect pairing, *J. Biol. Chem. 282*, 13573-13584.
48. Silverman, A. P., Jiang, Q., Goodman, M. F., and Kool, E. T. (2007) Steric and electrostatic effects in DNA synthesis by the SOS-induced DNA polymerases II and IV of Escherichia coli, *Biochemistry 46*, 13874-13881.
49. Lone, S., Townson, S. A., Uljon, S. N., Johnson, R. E., Brahma, A., Nair, D. T., Prakash, S., Prakash, L., and Aggarwal, A. K. (2007) Human DNA polymerase kappa encircles DNA: implications for mismatch extension and lesion bypass, *Mol. Cell. 25*, 601-614.
50. Pillaire, M. J., Betous, R., and Hoffmann, J. S. (2014) Role of DNA polymerase kappa in the maintenance of genomic stability, *Mol. Cell. Oncol. 1*, e29902.